bioRxiv preprint doi: https://doi.org/10.1101/691568; this version posted July 3, 2019. The copyright holder for this preprint (which was not certified by peer review) is the author/funder, who has granted bioRxiv a license to display the preprint in perpetuity. It is made available under aCC-BY 4.0 International license.

Title: Formation of Phage Lysis Patterns and Implications on Co-Propagation of Phages and Motile Host Bacteria

Xiaochu Li [1,2¶], Floricel Gonzalez [1¶], Nathaniel Esteves [1], Birgit E. Scharf [1*], Jing Chen [1*]

[1] Department of Biological Sciences, Virginia Polytechnic Institute and State University, Blacksburg, VA, 24060

[2] BIOTRANS Graduate Program, Virginia Polytechnic Institute and State University, Blacksburg, VA, 24060

* Corresponding authors: Email: chenjing@vt.edu (J.C.); bscharf@vt.edu (B.E.S.)

¶ These authors contributed equally to this work.

bioRxiv preprint doi: https://doi.org/10.1101/691568; this version posted July 3, 2019. The copyright holder for this preprint (which was not certified by peer review) is the author/funder, who has granted bioRxiv a license to display the preprint in perpetuity. It is made available under aCC-BY 4.0 International license.

Abstract

Coexistence of bacteriophages, or phages, and their host bacteria plays an important role in maintaining the microbial communities. In natural environments with limited nutrients, motile bacteria can actively migrate towards locations of richer resources. Although phages are not motile themselves, they can infect motile bacterial hosts and spread in space via the hosts. Therefore, in a migrating microbial community coexistence of bacteria and phages implies their co-propagation in space. Here, we combine an experimental approach and mathematical modeling to explore how phages and their motile host bacteria coexist and co-propagate. When lytic phages encountered motile host bacteria in our experimental set up, a sector-shaped lysis zone formed. Our mathematical model indicates that local nutrient depletion and the resulting inhibition of proliferation and motility of bacteria and phages are the key to formation of the observed lysis pattern. The model further reveals the straight radial boundaries in the lysis pattern as a tell-tale sign for coexistence and co-propagation of bacteria and phages. Emergence of such a pattern, albeit insensitive to extrinsic factors, requires a balance between intrinsic biological properties of phages and bacteria, which likely results from co-evolution of phages and bacteria.

bioRxiv preprint doi: https://doi.org/10.1101/691568; this version posted July 3, 2019. The copyright holder for this preprint (which was not certified by peer review) is the author/funder, who has granted bioRxiv a license to display the preprint in perpetuity. It is made available under aCC-BY 4.0 International license.

Author summary

Coexistence of phages and their bacterial hosts is important for maintaining the microbial communities. In a migrating microbial community, coexistence between phages and host bacteria implies that they co-propagate in space. Here we report a novel phage lysis pattern that is indicative of this co-propagation. The corresponding mathematical model we developed highlights a crucial dependence of the lysis pattern and implied phage-bacteria co-propagation on intrinsic properties allowing proliferation and spreading of the microbes in space. Remarkably, extrinsic factors, such as overall nutrient level, do not influence phage-bacteria coexistence and co-propagation. Findings from this work have strong implications for dispersal of phages mediated by motile bacterial communities, which will provide scientific basis for the fast-growing applications of phages.

bioRxiv preprint doi: https://doi.org/10.1101/691568; this version posted July 3, 2019. The copyright holder for this preprint (which was not certified by peer review) is the author/funder, who has granted bioRxiv a license to display the preprint in perpetuity. It is made available under aCC-BY 4.0 International license.

Introduction

Viruses that specifically target bacteria, bacteriophages or phages, are critical components of the microbial world. They are found in almost every natural environment, including soil, waters, oceans, and bodies of macroorganisms (e.g., human guts) [1-3]. Furthermore, they are the most abundant organisms in the biosphere [2]. Through their interactions with bacteria, phages constantly regulate the ecology, evolution, and physiology of microbial communities [1,2]. Because of their antimicrobial activity, the application of phages in food processing, agriculture, and medicine has exploded in recent years [4-6]. Development of these applications benefits from fundamental knowledge about how phages interact with bacteria in a microbial community and how they are dispersed in their microenvironment.

As obligate parasites of bacteria, phages must coexist with their hosts at the population level [1]. This coexistence, however, appears rather inconceivable because phages have a huge proliferative advantage over bacteria. The generation cycles of phage and bacteria fall in comparable time frames, with both the phage latent period and bacterial division cycle on the order of an hour [7]. But in each generation cycle a bacterium produces two daughter cells, while one phage produces ~100 new phage particles. Thus, it would follow that phages would quickly outnumber and annihilate the host bacterial population [8,9]. However, phages and bacteria have coexisted in natural environments for eons. Recent theoretical and experimental studies demonstrated that the evolutionary arms race could maintain coexistence of phages with host bacteria [10-13]. Coevolution could drive a phenotypic and genotypic diversity in the ability of phages to attack the bacteria and the ability of bacteria to resist the attacks, thereby maintaining the balance between phages and host bacteria [10,14-16]. However, for a successful evolutionary arms race, phages and bacteria need to coexist at least over the time scale required for the

bioRxiv preprint doi: https://doi.org/10.1101/691568; this version posted July 3, 2019. The copyright holder for this preprint (which was not certified by peer review) is the author/funder, who has granted bioRxiv a license to display the preprint in perpetuity. It is made available under aCC-BY 4.0 International license.

65 emergence of beneficial mutations [8,9]. It is therefore critical to understand the population
66 dynamics of phage-bacteria systems and conditions for their coexistence below the evolutionary
67 time scale.

68 Previous studies on coexistence of phages and bacteria mostly focused on well-mixed,
69 nearly homeostatic systems, such as cultures grown in chemostats [17-23]. Naturally occurring
70 systems of phages and bacteria, however, often do not satisfy the conditions found under these
71 defined laboratory settings. Firstly, natural systems typically do not offer a constant
72 environment. Unlike chemostats, where steady levels of nutrients and waste are maintained,
73 natural systems often experience sporadic deposition and replenishing of resources, and
74 fluctuations in other conditions. Secondly, natural systems usually exhibit spatial heterogeneity
75 to various degrees. The spatial inhomogeneity can significantly impact dynamical coexistence in
76 the phage-bacteria systems [8,9,24-26].

77 A critical spatial process in the phage-bacteria system is the migration of bacteria and
78 phages. Many motile bacteria can migrate towards nutrient-enriched areas via chemotaxis.
79 Phages themselves are not motile, so their dispersal relies on either passive diffusion or transport
80 by their hosts. However, diffusion is very inefficient for covering long distances. In addition,
81 diffusion of phage particles is typically reduced by higher bacterial densities and increased
82 viscosities due to bacterial exopolysaccharide production in biofilms [27-29]. Therefore, spatial
83 dispersal of phages mostly relies on infection of and transportation by their motile host bacteria.
84 It is poorly understood how phages and bacteria in a constantly migrating microbial community
85 achieve coexistence, which implies their co-propagation in space.

86 In this work we explored the co-propagation of phages and motile bacteria using a simple
87 experimental design, in which phages and bacteria were co-inoculated in a soft agar nutrient

bioRxiv preprint doi: https://doi.org/10.1101/691568; this version posted July 3, 2019. The copyright holder for this preprint (which was not certified by peer review) is the author/funder, who has granted bioRxiv a license to display the preprint in perpetuity. It is made available under aCC-BY 4.0 International license.

88 medium [30] (Fig 1a). The low agar concentration enabled motile bacteria to swim through the
89 matrix, which, in combination with bacterial growth, resulted in the formation of visible "swim
90 rings" [30]. Inoculation of bacteria and phages in separate locations allowed the experimental
91 setup to mirror realistic scenarios, in which expanding bacterial populations encounter phages in
92 a spatial domain. The described experiment generated a highly reproducible sector-shaped lysis
93 pattern. This pattern cannot be explained by any previous mathematical models describing phage
94 plaque formation [31-36], which inevitably produce circular patterns. Here we constructed a new
95 mathematical model for the spatial dynamics of phages and bacteria, which reproduced the
96 observed lysis pattern and revealed local nutrient depletion as the key to formation of the lysis
97 pattern. Moreover, our model revealed that the sector-shaped lysis pattern with straight radial
98 boundaries requires a balance between intrinsic biological properties of phages and bacteria, but
99 does not depend on extrinsic factors. Such a pattern was further shown to be a tell-tale sign for
100 extended spatial co-propagation of phages and bacteria, implying dependence of co-propagation
101 on intrinsic balance between phages and bacteria. This is the first time that a sector-shaped lysis
102 pattern has been reported in phage-bacteria systems. Our study of this phenomenon via an
103 integrated modeling and experimental approach provides critical insights into naturally occurring
104 dispersal and cohabitation of phages infecting motile bacteria.

bioRxiv preprint doi: https://doi.org/10.1101/691568; this version posted July 3, 2019. The copyright holder for this preprint (which was not certified by peer review) is the author/funder, who has granted bioRxiv a license to display the preprint in perpetuity. It is made available under aCC-BY 4.0 International license.

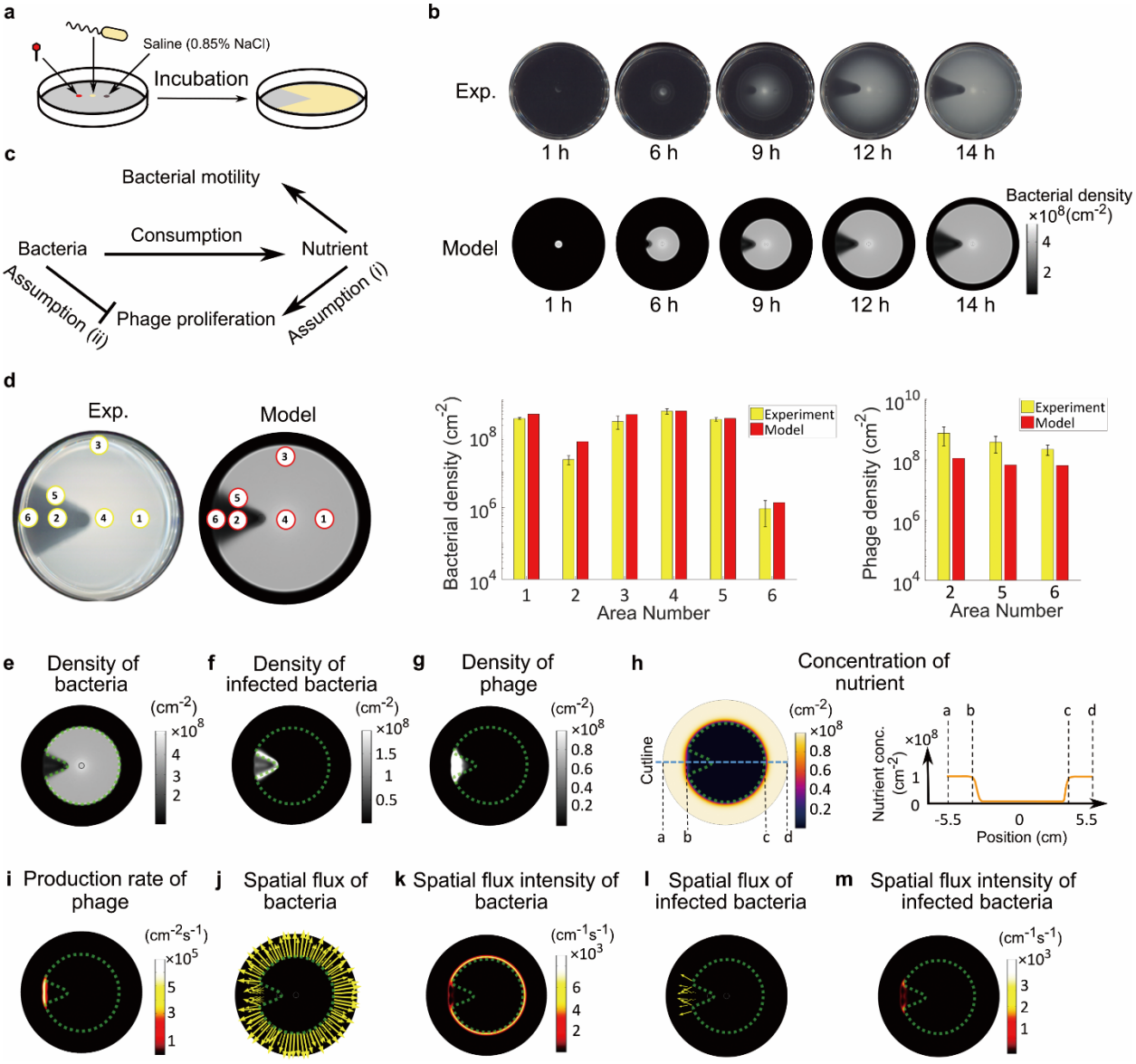

Figure 1. Sector-shaped lysis patterns emerge due to nutrient depletion. (a) Schematic of experimental procedure. Bacteria, phages, and a saline control were spotted on swim plates and incubated for 14 hours, which resulted in the development of the sector-shaped lysis pattern. (b) Experimental and model results of the lysis pattern over time. (c) Interactions between key processes in the model. Pointed arrows: positive influences. Blunt arrows: negative influences. (d) Quantitative comparison of bacterial and phage densities between experiment (yellow bars) and model (red bars). In the experiment, areas labeled by yellow numbers were sampled for phage and bacteria quantifications (see Methods). Corresponding areas in the model are labeled by red numbers. (e) Simulated density of total bacteria. The

bioRxiv preprint doi: https://doi.org/10.1101/691568; this version posted July 3, 2019. The copyright holder for this preprint (which was not certified by peer review) is the author/funder, who has granted bioRxiv a license to display the preprint in perpetuity. It is made available under aCC-BY 4.0 International license.

dashed green outline of the bacteria-dense area is superimposed on (f-m) for reference. (f) Simulated density of infected bacteria. (g) Simulated density of phages. (h) Simulated nutrient concentration (per unit area). Right: Orange curve shows the nutrient concentration profile along the axis of symmetry of the lysis pattern (blue dashed line in left panel). (i) Simulated phage production rate. Active phage production only happens at the outer edge of the lysis area. (j) Simulated spatial flux of total bacteria. (k) Intensity of bacterial spatial flux (~ length of arrow in (j)). Bacteria are motile only at the outer edge of the swim ring. (l) Simulated spatial flux of infected bacteria. (m) Intensity of spatial flux of infected bacteria (~ length of arrow in (l)). Infected bacteria are only motile at the outer edge of the lysis area. The spatial flux shown in (j-m) represents the sum of diffusion flux and chemotaxis flux. Length of the arrow is proportional to magnitude of the spatial flux. (e-m) present snapshots of model simulation at 10 h, an intermediate time at which the colony expansion and pattern formation progress steadily.

Results

Nutrient depletion is critical for formation of the lysis pattern

We designed a series of quantitative experiments based on our previously described phage drop assay [41], which allowed a spatially propagating bacterial population to encounter phages. *Salmonella enterica* serovar typhimurium 14028s and χ phage were inoculated 1 cm apart (Fig 1a) on 0.3% agar plate containing bacterial growth medium [30,42]. As the bacterial population grew, nutrients were consumed. Due to the low agar concentration, bacteria swam through the matrix and followed the self-generated nutrient gradient via chemotaxis, causing spreading of the bacterial population and the appearance of a swim ring. As the bacterial swim ring expanded, it reached the phage inoculation point. The phages then infected the bacteria and generated a lysis area with low bacterial density in the swim ring (Fig 1b). This experiment gave rise to an intriguing sector-shaped lysis pattern (Fig 1b). Most strikingly, as the bacterial swim

bioRxiv preprint doi: https://doi.org/10.1101/691568; this version posted July 3, 2019. The copyright holder for this preprint (which was not certified by peer review) is the author/funder, who has granted bioRxiv a license to display the preprint in perpetuity. It is made available under aCC-BY 4.0 International license.

ring expanded, the radial boundaries of the lysis area stayed unchanged behind the expanding front, resulting in a frozen or immobilized lysis pattern (Fig 1b, S1 Movie). Once the spreading of the swim ring stopped at the plate wall, the lysis pattern persisted for at least 48 hours (data not shown).

To understand the formation of this lysis pattern, we constructed a mean-field partial differential equation (PDE) model for the phage-bacteria system (Eqs.(1) ~ (4)). Like the previous phage plaque models [31-36], our model depicted the basic processes underlying the proliferation and propagation of phages and bacteria. Namely, the bacteria consume nutrients, divide, and move up the nutrient gradient via chemotaxis-directed swimming motility. Once infected by phages, the bacterium is lysed after a latent period, and release new phage progeny. Note that the run-and-tumble mechanism of bacterial chemotaxis results in a biased random walk of cells up the nutrient gradient. The random walk was expressed in the model as the cell diffusion terms and the bias as the cell drift terms (Eqs.(1) and (2)). In addition, we incorporated the following new assumptions about phage-bacteria interactions in the model, which were critical elements for formation of the sector-shaped lysis pattern (S1 Fig).

(i) Nutrient deficiency inhibits phage replication (Fig 1c). Because phage replication in the host bacteria requires energy, it is likely reduced at low nutrient levels.

(ii) High bacterial density inhibits phage production (Fig 1c). Such an effect has previously been implied in *Escherichia coli* and phage λ [43]: *E. coli* cells reduce the number of phage receptors in response to externally applied quorum sensing signals, resulting in decrease of phage adsorption rate and ultimately overall phage production.

Our model was able to reproduce the lysis pattern observed in the phage drop assay (Fig 1b, S1 Movie) and quantitatively match the bacterial and phage density profiles throughout

bioRxiv preprint doi: https://doi.org/10.1101/691568; this version posted July 3, 2019. The copyright holder for this preprint (which was not certified by peer review) is the author/funder, who has granted bioRxiv a license to display the preprint in perpetuity. It is made available under aCC-BY 4.0 International license.

different areas of the agar plate (Fig 1d). Both, experimental and modeling results, displayed the highest bacterial density at the inoculation point (area 4), followed by areas outside the lysis sector (areas 1 and 3), the radial boundary of the lysis pattern (area 5), and in the middle of the lysis pattern (area 2). The lowest bacterial density was at the outer edge of the lysis sector (area 6). The predicted phage densities also matched the experimental values, with the highest number of phages localized in the middle of the lysis sector and the lowest number present at the edge of the swim ring near the wall of the plate (Fig 1d). It should be noted that the lysis area was not entirely void of bacteria. In both experimental and modeling results, a low density of bacteria remained within the lysis area. In the model, nearly all bacteria in this area were infected bacteria (Fig 1e & f). In reality, this subpopulation could also include phage-resistant bacteria, which was not encompassed in our current model.

The model results revealed local nutrient depletion as the key reason for the lysis pattern to immobilize behind the expanding front of the bacterial swim ring. As the swim ring expanded, nutrients were depleted within the ring (Fig 1h). Nutrient depletion inhibited both phage production (Fig 1i) and bacterial motility (Fig 1j-m). Note that phages relied on the infection of motile bacteria to propagate in space. The passive diffusion of phage particles ($D_P \sim 1\ \mu m^2 h^{-1}$) was negligible compared to the effective diffusion of bacteria resulting from run-and-tumble ($D_B \sim 10^5\ \mu m^2 h^{-1}$) (Table 1). Therefore, inhibition of bacterial motility, especially motility of the infected bacteria (Fig 1l & m), also hindered spatial propagation of phages. Together, the inhibition of phage production and propagation due to local nutrient depletion and reduction of bacterial motility resulted in immobilization of the lysis pattern at the interior of the bacterial swim ring. The lysis pattern only actively grew at the expanding front of the swim ring, where

bioRxiv preprint doi: https://doi.org/10.1101/691568; this version posted July 3, 2019. The copyright holder for this preprint (which was not certified by peer review) is the author/funder, who has granted bioRxiv a license to display the preprint in perpetuity. It is made available under aCC-BY 4.0 International license.

183 nutrient supply from the unoccupied periphery supported active phage production and

184 propagation (Fig 1i-m).

185 **Table 1:** Parameters of mathematical model.

Symbols	Meaning	Default values	Sources
D_{Bmax}	Maximum diffusion coefficient of bacterial population (effective diffusion coefficient when bacteria assume maximum motility, see Supplementary Materials)	5.25×10^5 μm^{2}h^{-1}	Estimated from cell velocity and tumbling frequency [44,53]
K_c	Nutrient level for half maximum cell motility	0.02 μm^{-2}	Fitting to experimental data *
α_c	Chemotactic efficiency (see Supplementary Material)	2	Fitting to experimental data *
D_P	Diffusion coefficient of phage particles	1 μm^{2}h^{-1}	Particle size ~ 0.1 or 0.05 μm; diffusion coefficient ~ 1/particle size
D_n	Diffusion coefficient of nutrient	4.5×10^6 μm^{2}h^{-1}	[54]
η	Phage adsorption rate constant	8×10^4 μm^{2}h^{-1}	[55,56]
β	Phage burst size	80	[57]
k_l	Lysis rate constant of infected bacteria (~ reciprocal of latency period)	2 μm^{-2}h^{-1}	[56,58]
g_{max}	Maximum division rate of bacteria	6 h^{-1}	Fitting to experimental data *
K_n	Half-saturation nutrient concentration for Monod growth law	0.1 μm^{-2}	Fitting to experimental data *
λ	Bacterial growth yield (ratio between quantity of produced bacteria and quantity of consumed nutrient)	0.2	Fitting to experimental data *
K_b	Bacteria density for half maximum phage adsorption rate	0.1 μm^{-2}	Fitting to experimental sector-shaped lysis pattern
B_0	Number of inoculated bacteria	1×10^7	Experimental setup
P_0	Number of inoculated phages	1.5×10^8	Experimental setup
n_0	Initial area density of nutrient	1 μm^{-2}	Normalized (K_c, K_n and λ scale with n_0)
r	Radius of inoculation circle of bacteria and phage	0.25 cm	Experimental setup
R	Radius of plate	5.5 cm	Experimental setup

186 * Fitting to experimentally observed expansion rate of bacterial swim ring.

187

188 **The lysis pattern reflects radial projection of phage initiation zone**

bioRxiv preprint doi: https://doi.org/10.1101/691568; this version posted July 3, 2019. The copyright holder for this preprint (which was not certified by peer review) is the author/funder, who has granted bioRxiv a license to display the preprint in perpetuity. It is made available under aCC-BY 4.0 International license.

Interestingly, the experiment presented a decrease in the angle of the lysis sector when phages were inoculated further away from the bacterial inoculation point and vice versa (Fig 2a). This observation was faithfully reproduced by our model (Fig 2a). The lysis patterns in these cases approximately reflected the radial projection from the bacterial inoculation point over an approximately 0.7 cm circle centered at the phage inoculation point (Fig 2a, cartoon). In the model, we found that this projected area roughly corresponded to the area occupied by phages when nutrients initially got depleted at the phage inoculation point (Fig 2a, 3rd and 4th rows, nutrient depleted to 5 % of initial level). We hereby termed this area the "phage initiation zone". The phage initiation zone marked the initialization of the steady expansion of the lysis pattern. After the phage initiation zone was established, the phage and bacterial densities at the expanding front remained at a steady level throughout the rest of the pattern formation (S2 Fig).

bioRxiv preprint doi: https://doi.org/10.1101/691568; this version posted July 3, 2019. The copyright holder for this preprint (which was not certified by peer review) is the author/funder, who has granted bioRxiv a license to display the preprint in perpetuity. It is made available under aCC-BY 4.0 International license.

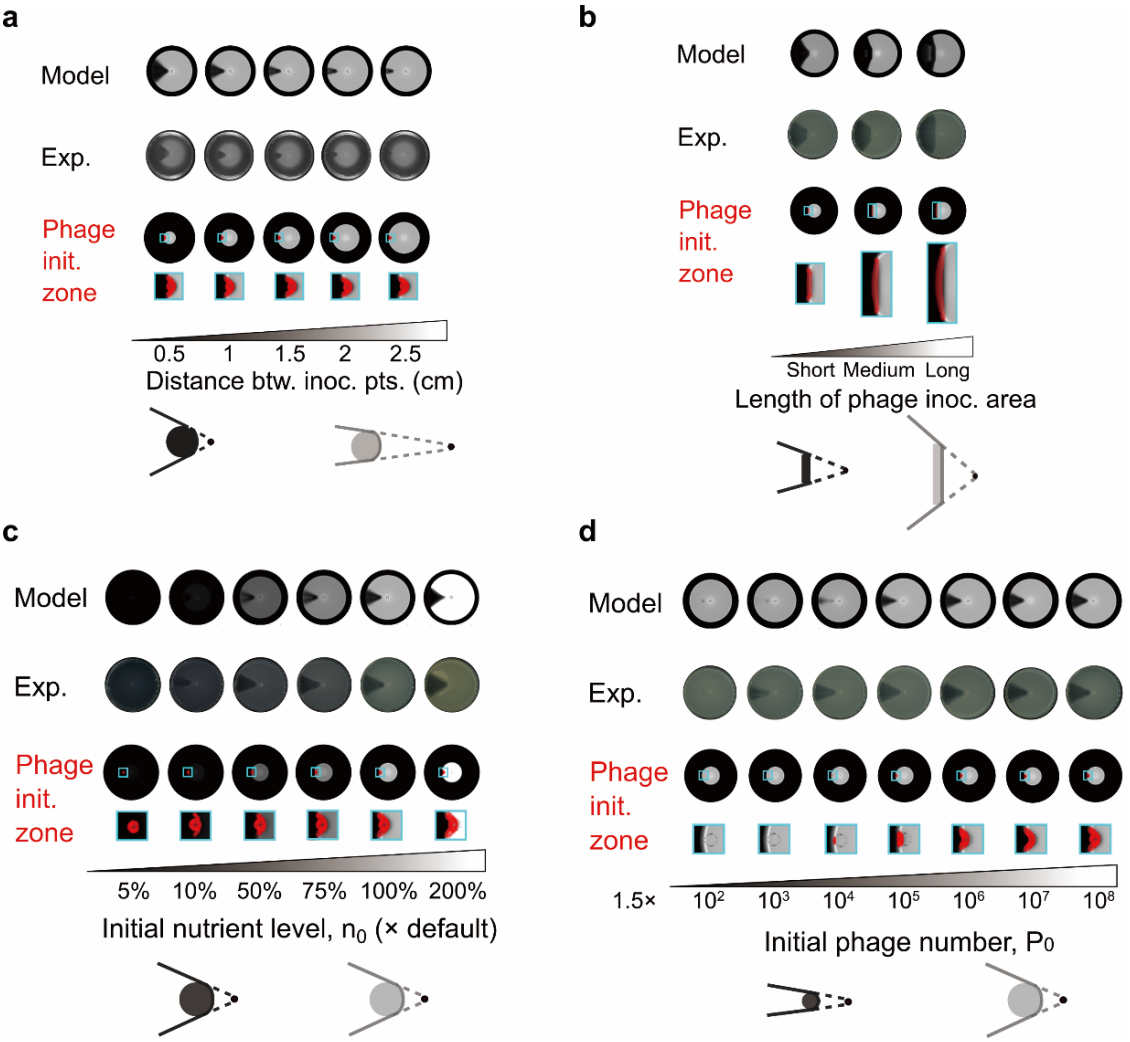

Figure 2. The lysis pattern reflects the radial projection of the phage initiation zone and is insensitive to extrinsic factors. Model and experimental results with (a) phages inoculated at different distances from the bacterial inoculation point, (b) phages inoculated with rods of different lengths, (c) different initial nutrient levels, and (d) different initial phage number. In (a-d), the phage initiation zones represent areas occupied by phages when the nutrient level at the center of the phage inoculation area drops below a certain threshold (set at 5 % of the initial nutrient level in model simulations). Cartoons summarize factors leading to different lysis patterns. Black dots: bacterial inoculation point. Solid dark grey and light grey areas: illustrative phage initiation zones. Solid lines: radial boundaries of lysis patterns. Dashed lines: extension from bacterial inoculation points to boundaries of the lysis areas.

bioRxiv preprint doi: https://doi.org/10.1101/691568; this version posted July 3, 2019. The copyright holder for this preprint (which was not certified by peer review) is the author/funder, who has granted bioRxiv a license to display the preprint in perpetuity. It is made available under aCC-BY 4.0 International license.

Our model further predicted how the phage initiation zone and the projected lysis pattern rely on additional factors. The predictions were all confirmed by experiments (Fig 2). Firstly, the phage initiation zone encompassed the original phage inoculation area (Fig 2a & b). Particularly, when phages were inoculated with rods that were significantly longer than the size of the phage initiation zone during point inoculation, the phage initiation zone became dominated by the rod size, and the lysis pattern roughly reflected the radial projection of the phage inoculation area (Fig 2b). Secondly, the size of the phage initiation zone remained roughly the same despite changes in total nutrient concentrations, resulting in similar angles of the lysis sector (Fig 2c). Thirdly, the phage initiation zone enlarged as initial phage particle number increased, resulting in a larger angle in the lysis sector (Fig 2d). Lower phage inoculation density led to decreased phage production and propagation by the time nutrient got depleted locally by bacteria. When initial phage numbers were too low, phages failed to establish the initiation zone, and subsequently, the lysis sector (Fig 2d, $P_0 = 1.5 \times 10^2$). The model also predicted that the initial bacteria number does not affect the lysis pattern (S3 Fig). Remarkably, the lysis pattern maintained straight radial boundaries (Fig 2) despite changes in the extrinsic factors tested above, i.e., distance between inoculation point, size of inoculation area, overall nutrient level, and initial phage/bacteria number.

Competition between phages and bacteria determines shape of lysis pattern

Although the straight radial boundaries of the lysis pattern were maintained under various external conditions like nutrient level and initial inoculation, our model predicted a significant change in the lysis pattern when intrinsic biological parameters were altered. In the simulation results, promoting the proliferative efficiency of phages (e.g., by increasing phage adsorption

bioRxiv preprint doi: https://doi.org/10.1101/691568; this version posted July 3, 2019. The copyright holder for this preprint (which was not certified by peer review) is the author/funder, who has granted bioRxiv a license to display the preprint in perpetuity. It is made available under aCC-BY 4.0 International license.

rate, phage burst size and lysis rate of infected bacteria) caused the lysis pattern to flare out, and decreasing phage proliferation caused the lysis pattern to close up (Fig 3, horizontal axes). Meanwhile, promoting bacterial proliferation caused the lysis pattern to curve inward and close up, and vice versa (Fig 3, vertical axes). In detail, the model assumed dependence of both bacterial and phage proliferation on nutrient (both are increasing functions of local nutrient concentration, see Materials and Methods). As previously shown, proliferation of bacteria caused nutrient to be depleted inside the bacterial swim ring (Fig 1h). Therefore, the bacterial proliferation rate at the expanding front determined how fast nutrients were depleted locally. This time further determined angular spreading of phages along the expanding front of the swim ring, because phage proliferation only thrived before nutrient was depleted locally. Therefore, either stronger phage proliferation or a weaker bacterial proliferation (causing slower nutrient consumption) allowed phages to spread in an accelerated fashion as the swim ring expanded, resulting in a flared-out lysis pattern. Vice versa, a weaker phage proliferation relative to bacterial proliferation resulted in a lysis pattern with edges closing inwards. The experimentally observed sector-shaped lysis pattern maintained straight radial boundaries despite changes in extrinsic variables, indicating that this observed pattern stemmed from a balance between proliferation of the bacterial and phage strains tested.

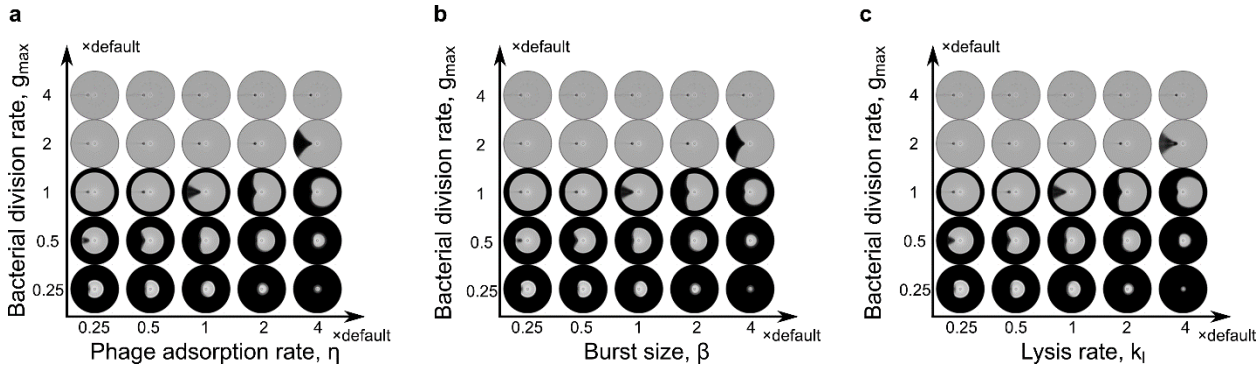

bioRxiv preprint doi: https://doi.org/10.1101/691568; this version posted July 3, 2019. The copyright holder for this preprint (which was not certified by peer review) is the author/funder, who has granted bioRxiv a license to display the preprint in perpetuity. It is made available under aCC-BY 4.0 International license.

Figure 3. Competition between bacterial and phage proliferation determines the shape of lysis patterns. Simulated lysis patterns with various bacterial growth rate constants versus (a) phage adsorption rate constants, (b) phage burst sizes, and (c) phage-induced lysis rate constants.

Bacterial motility and chemotaxis affects the lysis pattern

We next used the model to investigate how bacterial motility and chemotaxis influenced the shape of the lysis pattern. Bacterial motility was reflected by the bacterial diffusion coefficient in the model. A larger diffusion coefficient corresponds to higher cell speed [44]. Expectedly, a larger diffusion coefficient caused faster expansion of the bacterial swim ring in the model (Fig 4a). The chemotactic efficiency, on the other hand, characterized the bias of diffusion. Chemotaxis promoted the directed motility of bacteria in the radial direction due to the nutrient gradient formed by bacterial nutrient consumption (Fig 1h). Consistently, the model predicted that higher chemotactic efficiency expedites expansion of the bacterial swim ring (Fig 4a), because the moving cells at the expanding front can follow the nutrient gradient more efficiently.

bioRxiv preprint doi: https://doi.org/10.1101/691568; this version posted July 3, 2019. The copyright holder for this preprint (which was not certified by peer review) is the author/funder, who has granted bioRxiv a license to display the preprint in perpetuity. It is made available under aCC-BY 4.0 International license.

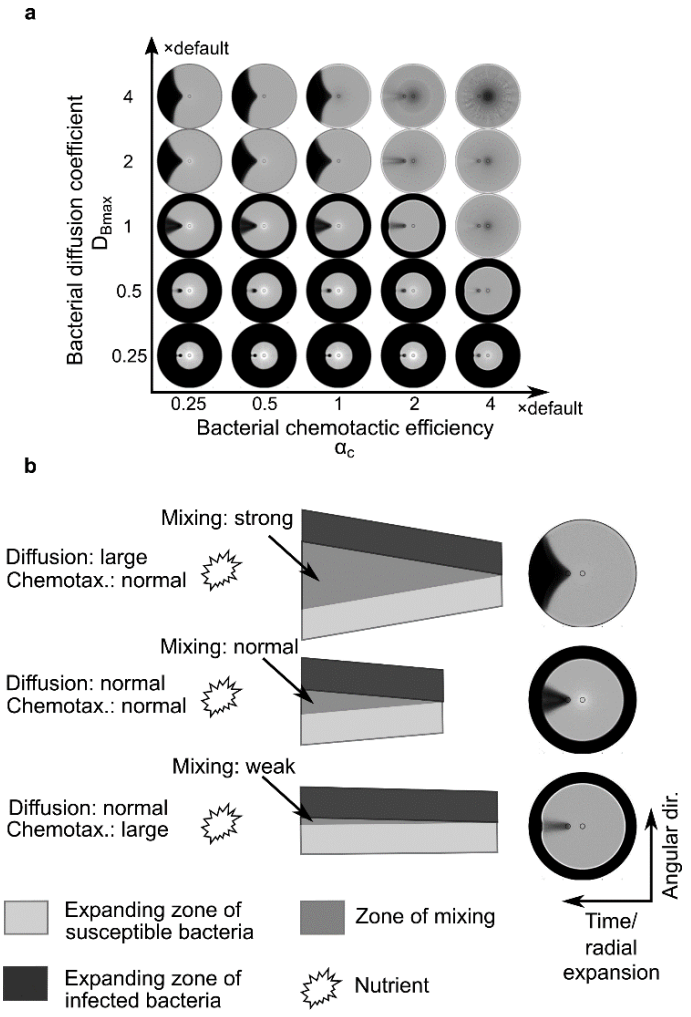

Figure 4. Effects of bacterial motility and chemotaxis on the shape of lysis patterns. (a) Simulated lysis patterns with various bacterial diffusion coefficients and chemotactic efficiencies. The diffusion coefficient in the model reflects the efficiency of bacterial motility. (b) Illustration of how bacterial diffusion and chemotaxis affect the evolution of lysis patterns. The cartoon illustrates a hypothetical history of expansion and mixing of two bacterial patches that would occur along the expanding front of the swim ring. Dark and light grey patch starts with infected and susceptible bacteria, respectively. Because nutrient is depleted behind the expanding front, bacterial expansion along the radial axis only occurs in the outward direction. Large bacterial diffusion promotes expansion equally in all directions, which enhances mixing between the infected and susceptible bacteria and leads to more effective phage propagation and flare-out of the lysis pattern (top row). In contrast, large chemotactic efficiency promotes

bioRxiv preprint doi: https://doi.org/10.1101/691568; this version posted July 3, 2019. The copyright holder for this preprint (which was not certified by peer review) is the author/funder, who has granted bioRxiv a license to display the preprint in perpetuity. It is made available under aCC-BY 4.0 International license.

278 expansion only against the nutrient gradient (radial direction), which effectively parallelizes bacterial
279 motion, reduces their mixing in the angular direction, and causes the lysis pattern to close up (bottom
280 row).
281
282 The effects of bacterial motility and chemotactic efficiency on the lysis pattern, however,
283 were predicted to be exactly opposite to each other. According to the simulation results,
284 increasing the bacterial diffusion coefficient or decreasing the chemotactic efficiency caused the
285 pattern to flare out (Fig 4a). Vice versa, decreasing the bacterial diffusion coefficient or
286 increasing chemotactic efficiency caused the pattern to close up (Fig 4a). The model generated
287 this result because increasing bacterial diffusion coefficient, i.e., increasing bacterial motility,
288 promoted mixing of infected and susceptible bacteria (Fig 4b, top row). Such mixing was critical
289 for spatial propagation of phages and angular expansion of the lysis pattern, because phages
290 could not move on their own and relied on infected bacteria to spread in space. In contrast,
291 enhancing chemotaxis inhibited such mixing, because it effectively promoted parallel motion of
292 the bacteria along the radial direction towards the high-nutrient area outside the swim ring (Fig
293 4b, bottom row). Taken together, bacterial motility and chemotaxis needed to be in balance to
294 generate a lysis pattern with straight radial boundaries. Collectively, these findings and those
295 from the model in the previous section indicated that bacterial motility and chemotaxis are
296 required to be in balance with bacterial and phage proliferation rate to generate straight radial
297 boundaries in the lysis pattern (S4 Fig).
298 To test the model predictions, we performed the phage drop assay with strains of *S.*
299 typhimurium 14028s containing deletions in two chemoreceptor encoding genes, *tar* and *tsr*.
300 Strains with deletions in *tar* or *tsr* did not significantly change the lysis pattern, whereas the
301 strain containing a deletion of both genes produced a moderate flare-out of the lysis pattern (S5

bioRxiv preprint doi: https://doi.org/10.1101/691568; this version posted July 3, 2019. The copyright holder for this preprint (which was not certified by peer review) is the author/funder, who has granted bioRxiv a license to display the preprint in perpetuity. It is made available under aCC-BY 4.0 International license.

Fig). This result was qualitatively consistent with the model prediction that weaker chemotactic efficiency caused a pattern with a wider angle (Fig 4a).

Straight radial boundary of lysis pattern is a tell-tale sign for extended co-propagation

A closer look at the model results revealed that the straight lysis pattern boundaries in the lysis pattern implied co-propagation of bacteria and phages over extended periods. Unlike the sector-shaped pattern with straight radial boundaries, a flared-out or closed-up lysis pattern indicated that one species would outcompete the other during the co-propagation (Fig 5a). For example, the result at the upper right corner of Fig 5a shows a case where phages encircled bacteria and blocked their further propagation in space. Vice versa, the result at the lower left corner of Fig 5a shows the opposite case where phage propagation was blocked by bacteria. For the less extreme flared-out or closed-up lysis patterns (e.g. upper left and lower right corners of Fig 5a), one species would eventually encircle and block the other, if the simulation had been run on a larger spatial domain that allowed further spatial expansion.

bioRxiv preprint doi: https://doi.org/10.1101/691568; this version posted July 3, 2019. The copyright holder for this preprint (which was not certified by peer review) is the author/funder, who has granted bioRxiv a license to display the preprint in perpetuity. It is made available under aCC-BY 4.0 International license.

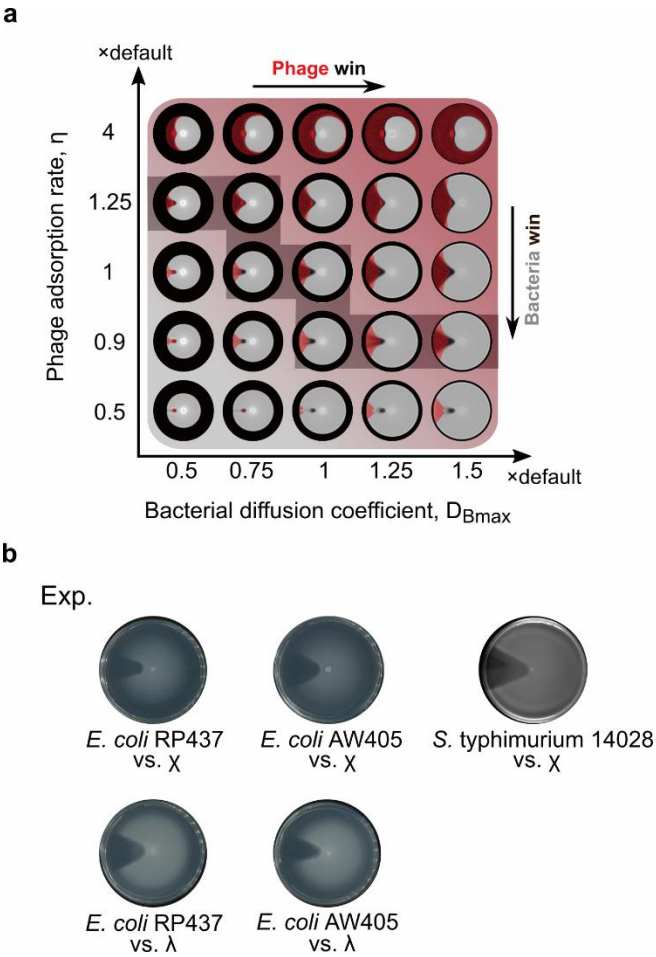

Figure 5. Co-propagation between phage and bacteria is reflected by the straight radial boundary of lysis pattern. (a) Lysis patterns and corresponding distribution of phages with various bacterial diffusion coefficients and phage adsorption rate constants. Red shade: density of phages. Grey shade: density of bacteria. Grey shadow staircase: potential trajectory of evolutionary arms race. (b) Experimental results from pairs of different bacterial species and their cognate phages.

Remarkably, similar sector-shaped lysis patterns with straight radial boundaries were observed in different bacteria-phage pairs (Fig 5b). First, we performed the phage drop assay using *E. coli* and phage χ, and found a similar sector-shaped lysis pattern (Fig 5b, first row). Since χ is a bacterial flagella-dependent phage [45-47], we further examined whether infection of motile *E. coli* by a non-flagellotropic phage, λ, would generate a similar lysis pattern. Phage λ

bioRxiv preprint doi: https://doi.org/10.1101/691568; this version posted July 3, 2019. The copyright holder for this preprint (which was not certified by peer review) is the author/funder, who has granted bioRxiv a license to display the preprint in perpetuity. It is made available under aCC-BY 4.0 International license.

329 was chosen because of an overlapping bacterial host range with χ. Interestingly, similar sector-
330 shaped lysis patterns were observed independent of the utilized phage type (Fig 5b). Combined
331 with the model findings above and earlier results on sensitivity of the pattern to intrinsic
332 parameters, these highly similar sector-shaped lysis patterns indicated that both *Salmonella* and
333 *E. coli* achieved intrinsic biological balance with both phages, λ and χ.
334

335 ## Discussion

336 In this work, we combined experiments and modeling of lysis pattern formation to
337 investigate the coexistence and co-propagation of phages and bacteria in space. Our experimental
338 setting has strong implications for realistic scenarios, where an expanding bacterial population
339 encounters phages and mediates their dispersal. We observed the formation of an asymmetric,
340 sector-shaped lysis pattern, which cannot be explained by previous models for lysis pattern
341 formation in phage-bacteria systems. Our new mathematical model successfully reproduced the
342 experimental observation and revealed the importance of nutrient depletion in maintaining the
343 geometric asymmetry initialized in the system. Specifically, local nutrient depletion inhibited
344 phage production and propagation behind the expanding front of the bacterial swim ring, thus
345 immobilizing the lysis pattern. Without the immobilization effect, the lysis pattern would lose
346 asymmetry and eventually reduce to a circle, as predicted by the previous models for phage
347 plaque formation [31-36].
348 Most importantly, straight radial boundaries of the lysis pattern presented a tell-tale sign
349 that a phage-bacteria system is capable of co-propagation over extended period (Fig 5a).
350 Therefore, the shape of the lysis pattern can serve as a reporter of co-propagation. The model
351 further demonstrated that a straightly expanding pattern requires balance between bacterial and

bioRxiv preprint doi: https://doi.org/10.1101/691568; this version posted July 3, 2019. The copyright holder for this preprint (which was not certified by peer review) is the author/funder, who has granted bioRxiv a license to display the preprint in perpetuity. It is made available under aCC-BY 4.0 International license.

phage proliferation efficiency, and bacterial motility and chemotaxis (Figs 3, 4 and S4 Fig). The balance of biological properties keeps angular expansion of the lysis pattern in pace with its radial expansion and creates straight radial boundaries in the evolving lysis pattern. In contrast, the straight boundary is insensitive to extrinsic factors, such as nutrient levels and initial phage/bacterial numbers (Fig 2, S3 and S6 Figs). Together, these findings suggest that balance of intrinsic factors supports robust co-propagation of phages and bacteria regardless of variations in the environment or initial conditions. Interestingly, we experimentally discovered similar sectorial lysis patterns with straight radial boundaries in two different enteric bacterial species paired with two different phages (Fig 5b). These lysis patterns implied intrinsic biological balance between the phages and their bacterial hosts. This phenomenon suggests that natural pairs of bacteria and phages could have shaped their biological properties to allow robust spatial coexistence and co-propagation, likely as a result of coevolution. In the future, we will perform the phage drop assay on other phage-bacteria pairs to examine whether this conclusion may be generalized universally.

The model predictions on extrinsic factors were verified by our experiments (Fig 2). It was much more complicated, though, to vary the intrinsic biological properties in a controlled fashion. We are relegating these experimental testing to future work, which will also provide feedback for model refinement. For example, the predicted lysis pattern only changed significantly when chemotactic efficiency was increased from the default value (Fig 4a), whereas a flared-out lysis pattern occurred experimentally in a strain lacking two major chemoreceptors (S5 Fig). This quantitative discrepancy indicates that the chemotaxis term and/or parameters in the model should be modified in the future.

bioRxiv preprint doi: https://doi.org/10.1101/691568; this version posted July 3, 2019. The copyright holder for this preprint (which was not certified by peer review) is the author/funder, who has granted bioRxiv a license to display the preprint in perpetuity. It is made available under aCC-BY 4.0 International license.

Our study specifically underscores the importance of co-propagation of phages and bacteria, i.e., their coexistence in the context of a migrating microbial community. We found that co-propagation requires not only a balance between the proliferative efficiency of phages and bacteria, but also between their ability to spread in space (autonomous spreading of bacteria vs. bacteria-mediated spreading of phages). The requirement of balanced proliferative efficiency is known to create the selective pressure that drives the evolutionary arms race between phages and bacteria in their ability to attack and resist attack [10,12,14-16]. Similarly, the requirement of balanced ability to spread in space could also create a selective pressure to drive an arms race in evolving stronger ability to spread in space (Fig 5a, dark shaded staircase). For example, the emergence of flagellotropic phages, i.e., phages specifically targeting actively rotating bacterial flagella [48], could reflect an evolved strategy for phages to improve their ability to propagate in space. Interestingly, our model demonstrates a significant impact of chemotactic efficiency on co-propagation of phages and bacteria (Fig 4 and S6d Fig). Therefore, bacteria could theoretically evolve higher chemotactic efficiency as a counterattack on phage infection. In the future we will examine whether the arms race between phages and bacteria indeed affect the diversity in genes regulating bacterial chemotaxis.

Our current work exploited the simplest possible experimental and model setup to understand how phages and bacteria coexist and co-propagate in space, using lytic phages and uniform initial nutrient concentration. In the future, we will modify our experimental and model parameters to investigate additional factors, such as lysogeny and non-uniform nutrient distribution, on the spatial dynamics of phages and bacteria. We will also incorporate coevolution between phages and bacteria into our model and experimental set up, to investigate the long-term co-propagation under the effect of evolution. Findings from this work have strong

bioRxiv preprint doi: https://doi.org/10.1101/691568; this version posted July 3, 2019. The copyright holder for this preprint (which was not certified by peer review) is the author/funder, who has granted bioRxiv a license to display the preprint in perpetuity. It is made available under aCC-BY 4.0 International license.

implications for dispersal of phages in microbial communities and lay the groundwork for future applications, such as phage therapy. Ultimately, we hope to create a model that will aid successful selection and engineering of phages for targeted applications by providing information on phage dispersal and interaction with host bacteria in the corresponding environment.

Materials and Methods

Bacterial strains and phages. The strains of bacteria and phages used are listed in Table 2.

Table 2: Biological materials used in this study.

Species/strains/ plasmids	Relevant characteristics	Sources	References
Salmonella enterica serovar typhimurium			
14028s	Wild type	Gift from Rasika M. Harshey	
14028s Tar$^-$	*tar*$^-$	This work	
14028s Tsr$^-$	*tsr*$^-$	This work	
RH2312/SM20	*tar*$^-$*tsr*$^-$	Gift from Rasika M. Harshey	
TH2788	*fliY*5221::Tn*10d*Tc (−86 from ATG of *fliY*)	Gift from Kelly T. Hughes	
Agrobacterium sp. H13-3			
RU12/001	Sm^r; spontaneous streptomycin resistant wild-type strain		[49]
Escherichia coli			
RP437	Wild type	Gift from Howard C. Berg	[50]
AW405	Wild type	Gift from Howard C. Berg	[51]
Phages			
λ phage	*vir*	Gift from Rüdiger Schmitt	[52]
χ phage		Gift from Kelly T. Hughes	
Plasmid			
pKD46	*bla* P_{BAD} *gam beto exo* pSC101 *oriTS*	Gift from Howard C. Berg	[37]

bioRxiv preprint doi: https://doi.org/10.1101/691568; this version posted July 3, 2019. The copyright holder for this preprint (which was not certified by peer review) is the author/funder, who has granted bioRxiv a license to display the preprint in perpetuity. It is made available under aCC-BY 4.0 International license.

Media and growth conditions. *Salmonella enterica* serovar Typhimurium 14028s was grown in MSB at 37 °C. MSB is a modified LB medium (1 % tryptone, 0.5 % yeast extract, and 0.5 % NaCl) supplemented with 2 mM $MgSO_4$ and 2 mM $CaCl_2$. *Escherichia coli* strains were grown at 30 °C in T-broth containing 1 % tryptone and 0.5 % NaCl at 30 °C.

Construction of mutant strains. The protocol for lambda-Red genetic engineering [37,38] was followed to make *S.* typhimurium mutant lacking *tar*.

Phage drop assay. Swim plates containing MSB medium (for *S.* Typhimurium) or T-broth (for *E. coli*) and 0.3% bacto agar were inoculated with 2.5 µl of a stationary phase bacterial culture in the center of the plate along with 2.5 µl of phage suspension (MOI = 25.4) at a 1 cm distance from the inoculation point. A 2.5 µl spot of 0.85% saline was placed at the same distance from the bacterial inoculation point, opposite from the phage suspension, as a control. pPlates were incubated at 37 °C (*S.* Typhimurium) or 30 °C (*E. coli*) for 14 hours. All plates were imaged using the Epson Perfection V370 scanner. Phage drop assays with slight modifications were conducted to test different variables. For the rod shaped inoculations, sealed glass capillaries of different lengths were immersed in phage suspension and pressed against the soft agar at a distance of 0.5 cm from the bacterial inoculation point. To test the effect of varying inoculation distances, phage suspensions were inoculated at 0.5, 1.0, 1.5, 2.0, and 2.5 cm from the bacterial inoculation point. For altered nutrient concentration experiments, the initial concentrations of tryptone and yeast extract were adjusted to be 0.05, 0.1, 0.5, 0.75, or 2.0 times of the regular nutrient concentration, which is referred to as a concentration of 1. To evaluate the effect of phage number, the initial phage stock was serially diluted ten-fold and then spotted on the plate. In experiments conducted with λ phage, the swim plates were supplemented with 10 mM $MgSO_4$ and 0.2 % maltose.

bioRxiv preprint doi: https://doi.org/10.1101/691568; this version posted July 3, 2019. The copyright holder for this preprint (which was not certified by peer review) is the author/funder, who has granted bioRxiv a license to display the preprint in perpetuity. It is made available under aCC-BY 4.0 International license.

Phage titer. Serial dilutions of the phage stock were made and 100 µl of each dilution was added to host bacterial cells with an OD_{600} of 1.0. Bacteria-phage mixtures were incubated for 10 min at room temperature. Each mix received 4 ml of pre-heated 0.5 % soft agar and was then overlaid on LB plates. Plates were incubated at 37 °C for 4-6 h. The titer of the phage stock was determined by counting the plaques on the plate that yielded between 30 to 300 plaque forming units and multiplying the number by the dilution factor.

χ phage preparation. Dilutions of phage suspensions mixed with bacteria were plated to achieve confluent lysis as described in the phage titer protocol using 0.35 % agar for the overlay. Following formation of plaques, 5 ml of TM buffer (20 mM Tris/HCl [pH=7.5], 10 mM $MgSO_4$) was added to each plate and incubated on a shaking platform at 4 °C for a minimum of 6 h. The soft agar/buffer mixture was collected, pooled, and bacteria were lysed by adding chloroform to at final concentration of 0.02 %. Samples were mixed vigorously for 1 min, transferred to glass tubes, and centrifuged at 10,000 x g for 15 min at room temperature. The supernatant was passed through a 0.45 µm filter and NaCl was added to a final concentration of 4 %. The protocol of phage preparation was followed as described in [39]. The final phage stock was stored in TM buffer at 4 °C.

Bacteria and phage quantifications. Phage drop assays were conducted as described above. At the 14-hour end point, different areas of the plate were sampled by taking agar plugs using a 10 ml syringe barrel with plunger. Each agar plug was placed in 1 ml of 0.85 % saline and incubated at room temperature for 10 min with shaking to allow even mixture of the agar. Serial dilutions of each sample were plated on LB agar plates and incubated at 37 °C overnight. For phage quantifications, 100 µl of chloroform was added to each sample. The number of phage particles present in each sample was quantified as described in the phage titer protocol. Densities

bioRxiv preprint doi: https://doi.org/10.1101/691568; this version posted July 3, 2019. The copyright holder for this preprint (which was not certified by peer review) is the author/funder, who has granted bioRxiv a license to display the preprint in perpetuity. It is made available under aCC-BY 4.0 International license.

453 reported correspond to plaque forming units (for phage) or colony forming units (for bacteria).
454 To compare with model results, the volume densities were converted to area densities, based on
455 0.5 cm thickness in the agar, i.e., area density (cm^{-2}) = volume density (CFU/cm^3 or PFU/cm^3) ×
456 0.5 cm.

457 **Model setup.** We constructed a mean-field diffusion-drift-reaction model for the
458 bacteria-phage system. Our model includes four variables: density of susceptible bacteria
459 $B(x,t)$, density of infected bacteria $L(x,t)$, density of phages $P(x,t)$, and nutrient concentration
460 $n(x,t)$. The state variables and parameters are summarized in Table 1. The equations governing
461 the spatiotemporal dynamics of bacteria, phages and nutrient read as Eqs. (1) ~ (4).

462 Susceptible bacteria:

$$\frac{\partial B}{\partial t} = \underbrace{D_{Bmax}\nabla\left[\left(\frac{n}{n+K_c}\right)\nabla B\right]}_{\text{cell diffusion}} - \underbrace{D_{Bmax}\alpha_c\nabla\left[\frac{K_c}{(n+K_c)^2}B\nabla n\right]}_{\text{cell drift}} - \underbrace{\eta\frac{K_b}{B+L+K_b}BP}_{\text{phage adsorption}} + \underbrace{g_{max}\frac{n}{n+K_n}B}_{\text{cell division}} \quad (1)$$

463 Infected bacteria:

$$\frac{\partial L}{\partial t} = \underbrace{D_{Bmax}\nabla\left[\left(\frac{n}{n+K_c}\right)\nabla L\right]}_{\text{cell diffusion}} - \underbrace{D_{Bmax}\alpha_c\nabla\left[\frac{K_c}{(n+K_c)^2}L\nabla n\right]}_{\text{cell drift}} + \underbrace{\eta\frac{K_b}{B+L+K_b}BP}_{\text{phage adsorption}} - \underbrace{k_l Ln}_{\text{cell lysis}} \quad (2)$$

464 Phages:

$$\frac{\partial P}{\partial t} = \underbrace{D_P\nabla^2 P}_{\text{phage diffusion}} - \underbrace{\eta\frac{K_b}{B+L+K_b}(L+B)P}_{\text{phage multi-adsorption}} + \underbrace{\beta k_l Ln}_{\text{phage bursting}} \quad (3)$$

465 Nutrient:

bioRxiv preprint doi: https://doi.org/10.1101/691568; this version posted July 3, 2019. The copyright holder for this preprint (which was not certified by peer review) is the author/funder, who has granted bioRxiv a license to display the preprint in perpetuity. It is made available under aCC-BY 4.0 International license.

$$\frac{\partial n}{\partial t} = \underbrace{D_n \nabla^2 n}_{\text{nutrient diffusion}} - \underbrace{\lambda g_{max} \frac{n}{n + K_n} (B + L)}_{\text{nutrient consumption by bacteria}} \quad (4)$$

Eqs. (1) ~ (4) incorporate the following model assumptions.

(1) The division rate of susceptible bacteria follows the Monod rate law [40].

(2) Division of the infected bacteria is neglected because they are likely lysed before dividing. But they consume nutrients at the same rate as susceptible bacteria (changing this rate does not affect the qualitative behavior of the model).

(3) The phage adsorption rate decreases with increasing bacterial density. This is how New Assumption (ii) in Results is implemented.

(4) Multi-adsorption is considered, i.e., phages can be adsorbed onto bacteria that are already infected.

(5) Because phage assembly requires energy, we assume that the lysis period elongates as nutrient level decreases. This is how New Assumption (i) in Results is implemented.

(6) Because bacterial motility requires energy, it depends on nutrient level. This dependence is reflected in both the diffusion and chemotaxis terms. Derivation of the diffusion and chemotaxis terms is given in the Supplementary Materials and S7 Fig. Both susceptible and infected bacteria follow these spatial dynamics.

Acknowledgements

We thank Kelly T. Hughes for the gift of χ phage, Rüdiger Schmitt for λ phage, Howard C. Berg for providing us with pKD46 and various *E. coli* strains, Rasika M. Harshey for the gift of the *Salmonella* strains, and Elizabeth Denson for creating the *Salmonella* typhimurium strain lacking

bioRxiv preprint doi: https://doi.org/10.1101/691568; this version posted July 3, 2019. The copyright holder for this preprint (which was not certified by peer review) is the author/funder, who has granted bioRxiv a license to display the preprint in perpetuity. It is made available under aCC-BY 4.0 International license.

the *tar* gene. We thank Dilara Long for contributing to simulations of an earlier version of the model.

References

1 Salmond, G. P. & Fineran, P. C. A century of the phage: past, present and future. *Nat Rev Microbiol* **13**, 777-786, doi:10.1038/nrmicro3564 (2015).

2 Clokie, M. R., Millard, A. D., Letarov, A. V. & Heaphy, S. Phages in nature. *Bacteriophage* **1**, 31-45, doi:10.4161/bact.1.1.14942 (2011).

3 Bergh, O., Borsheim, K. Y., Bratbak, G. & Heldal, M. High abundance of viruses found in aquatic environments. *Nature* **340**, 467-468, doi:10.1038/340467a0 (1989).

4 Svircev, A., Roach, D. & Castle, A. Framing the future with bacteriophages in agriculture. *Viruses* **10**, doi:10.3390/v10050218 (2018).

5 Chan, B. K., Turner, P. E., Kim, S., Mojibian, H. R., Elefteriades, J. A. & Narayan, D. Phage treatment of an aortic graft infected with *Pseudomonas aeruginosa*. *Evol Med Public Health* **2018**, 60-66, doi:10.1093/emph/eoy005 (2018).

6 Ly-Chatain, M. H. The factors affecting effectiveness of treatment in phages therapy. *Front Microbiol* **5**, 51, doi:10.3389/fmicb.2014.00051 (2014).

7 Milo, R., Jorgensen, P., Moran, U., Weber, G. & Springer, M. BioNumbers--the database of key numbers in molecular and cell biology. *Nucleic Acids Res* **38**, D750-753, doi:10.1093/nar/gkp889 (2010).

8 Heilmann, S., Sneppen, K. & Krishna, S. Sustainability of virulence in a phage-bacterial ecosystem. *J Virol* **84**, 3016-3022, doi:10.1128/JVI.02326-09 (2010).

9 Heilmann, S., Sneppen, K. & Krishna, S. Coexistence of phage and bacteria on the boundary of self-organized refuges. *Proc Natl Acad Sci U S A* **109**, 12828-12833, doi:10.1073/pnas.1200771109 (2012).

10 Koskella, B. & Brockhurst, M. A. Bacteria-phage coevolution as a driver of ecological and evolutionary processes in microbial communities. *Fems Microbiology Reviews* **38**, 916-931, doi:10.1111/1574-6976.12072 (2014).

11 Rodriguez-Valera, F., Martin-Cuadrado, A. B., Rodriguez-Brito, B., Pasic, L., Thingstad, T. F., Rohwer, F. *et al.* Explaining microbial population genomics through phage predation. *Nature Reviews Microbiology* **7**, 828-836, doi:10.1038/nrmicro2235 (2009).

12 Weitz, J. S., Hartman, H. & Levin, S. A. Coevolutionary arms races between bacteria and bacteriophage. *Proceedings of the National Academy of Sciences of the United States of America* **102**, 9535-9540, doi:10.1073/pnas.0504062102 (2005).

13 Haerter, J. O., Mitarai, N. & Sneppen, K. Phage and bacteria support mutual diversity in a narrowing staircase of coexistence. *ISME J* **8**, 2317-2326, doi:10.1038/ismej.2014.80 (2014).

14 Abedon, S. T. *Bacteriophage Ecology: Population Growth, Evolution, and Impact of Bacterial Viruses*. (Cambridge University Press, 2008).

15 Wright, R. C. T., Friman, V. P., Smith, M. C. M. & Brockhurst, M. A. Cross-resistance is modular in bacteria-phage interactions. *Plos Biology* **16**, doi:10.1371/journal.pbio.2006057 (2018).

bioRxiv preprint doi: https://doi.org/10.1101/691568; this version posted July 3, 2019. The copyright holder for this preprint (which was not certified by peer review) is the author/funder, who has granted bioRxiv a license to display the preprint in perpetuity. It is made available under aCC-BY 4.0 International license.

16 Stern, A. & Sorek, R. The phage-host arms race: shaping the evolution of microbes. *Bioessays* **33**, 43-51, doi:10.1002/bies.201000071 (2011).
17 Campbell, A. Conditions for existence of bacteriophage. *Evolution* **15**, 153-&, doi:Doi 10.2307/2406076 (1961).
18 Levin, B. R., Stewart, F. M. & Chao, L. Resource-limited growth, competition, and predation - a model and experimental studies with bacteria and bacteriophage. *Am Nat* **111**, 3-24, doi:Doi 10.1086/283134 (1977).
19 Smith, H. L. & Trevino, R. T. Bacteriophage infection dynamics: multiple host binding sites. *Math Model Nat Pheno* **4**, 109-134, doi:10.1051/mmnp/20094604 (2009).
20 Smith, H. L. Models of virulent phage growth with application to phage therapy. *Siam Journal on Applied Mathematics* **68**, 1717-1737, doi:10.1137/070704514 (2008).
21 Kasman, L. M., Kasman, A., Westwater, C., Dolan, J., Schmidt, M. G. & Norris, J. S. Overcoming the phage replication threshold: a mathematical model with implications for phage therapy. *Journal of Virology* **76**, 5557-5564, doi:10.1128/Jvi.76.11.5557-5564.2002 (2002).
22 Santos, S. B., Carvalho, C., Azeredo, J. & Ferreira, E. C. Population dynamics of a Salmonella lytic phage and its host: implications of the host bacterial growth rate in modelling. *PLoS One* **9**, e102507, doi:10.1371/journal.pone.0102507 (2014).
23 Beretta, E. & Kuang, Y. Modeling and analysis of a marine bacteriophage infection with latency period. *Nonlinear Anal-Real* **2**, 35-74, doi:10.1016/S0362-546x(99)00285-0 (2001).
24 Schrag, S. J. & Mittler, J. E. Host-parasite coexistence: The role of spatial refuges in stabilizing bacteria-phage interactions. *Am Nat* **148**, 348-377, doi:Doi 10.1086/285929 (1996).
25 Brockhurst, M. A., Buckling, A. & Rainey, P. B. Spatial heterogeneity and the stability of host-parasite coexistence. *J Evol Biol* **19**, 374-379, doi:10.1111/j.1420-9101.2005.01026.x (2006).
26 Kerr, B., Neuhauser, C., Bohannan, B. J. & Dean, A. M. Local migration promotes competitive restraint in a host-pathogen 'tragedy of the commons'. *Nature* **442**, 75-78, doi:10.1038/nature04864 (2006).
27 Abedon, S. T., Kuhl, S. J., Blasdel, B. G. & Kutter, E. M. Phage treatment of human infections. *Bacteriophage* **1**, 66-85, doi:10.4161/bact.1.2.15845 (2011).
28 Chan, B. K. & Abedon, S. T. Bacteriophages and their enzymes in biofilm control. *Curr Pharm Design* **21**, 85-99 (2015).
29 Simmons, M., Drescher, K., Nadell, C. D. & Bucci, V. Phage mobility is a core determinant of phage-bacteria coexistence in biofilms. *Isme Journal* **12**, 532-543, doi:10.1038/ismej.2017.190 (2018).
30 Wolfe, A. J. & Berg, H. C. Migration of bacteria in semisolid agar. *Proc Natl Acad Sci U S A* **86**, 6973-6977 (1989).
31 Mitarai, N., Brown, S. & Sneppen, K. Population dynamics of phage and bacteria in spatially structured habitats using phage lambda and *Escherichia coli*. *J Bacteriol* **198**, 1783-1793, doi:10.1128/JB.00965-15 (2016).
32 Fort, J. A comment on amplification and spread of viruses in a growing plaque. *J Theor Biol* **214**, 515-518, doi:10.1006/jtbi.2001.2469 (2002).
33 You, L. & Yin, J. Amplification and spread of viruses in a growing plaque. *J Theor Biol* **200**, 365-373, doi:10.1006/jtbi.1999.1001 (1999).

bioRxiv preprint doi: https://doi.org/10.1101/691568; this version posted July 3, 2019. The copyright holder for this preprint (which was not certified by peer review) is the author/funder, who has granted bioRxiv a license to display the preprint in perpetuity. It is made available under aCC-BY 4.0 International license.

34 Yin, J. & McCaskill, J. S. Replication of viruses in a growing plaque: a reaction-diffusion model. *Biophys J* **61**, 1540-1549, doi:10.1016/S0006-3495(92)81958-6 (1992).

35 Gourley, S. A. & Kuang, Y. A delay reaction-diffusion model of the spread of bacteriophage infection. *Siam Journal on Applied Mathematics* **65**, 550-566, doi:10.1137/S0036139903436613 (2005).

36 Jones, D. A. & Smith, H. L. Bacteriophage and bacteria in a flow reactor. *Bulletin of Mathematical Biology* **73**, 2357-2383, doi:10.1007/s11538-010-9626-0 (2011).

37 Datsenko, K. A. & Wanner, B. L. One-step inactivation of chromosomal genes in *Escherichia coli* K-12 using PCR products. *Proceedings of the National Academy of Sciences of the United States of America* **97**, 6640-6645, doi:DOI 10.1073/pnas.120163297 (2000).

38 Karlinsey, J. E. Lambda-red genetic engineering in *Salmonella enterica* serovar typhimurium. *Advanced Bacterial Genetics: Use of Transposons and Phage for Genomic Engieering* **421**, 199-209, doi:10.1016/S0076-6879(06)21016-4 (2007).

39 Gonzalez, F., Helm, R. F., Broadway, K. M. & Scharf, B. E. More than rotating flagella: Lipopolysaccharide as a secondary receptor for flagellotropic phage 7-7-1. *Journal of Bacteriology* **200**, doi:10.1128/JB.00363-18 (2018).

40 Monod, J. The growth of bacterial cultures. *Annual Review of Microbiology* **3**, 371-394, doi:DOI 10.1146/annurev.mi.03.100149.002103 (1949).

41 Yen, J. Y., Broadway, K. M. & Scharf, B. E. Minimum requirements of flagellation and motility for infection of *Agrobacterium* sp. strain H13-3 by flagellotropic bacteriophage 7-7-1. *Appl Environ Microbiol* **78**, 7216-7222, doi:10.1128/AEM.01082-12 (2012).

42 Adler, J. Chemotaxis in bacteria. *Science* **153**, 708-&, doi:DOI 10.1126/science.153.3737.708 (1966).

43 Hoyland-Kroghsbo, N. M., Maerkedahl, R. B. & Lo Svenningsen, S. A quorum-sensing-induced bacteriophage defense mechanism. *Mbio* **4**, doi:10.1128/mBio.00362-12 (2013).

44 Patteson, A. E., Gopinath, A., Goulian, M. & Arratia, P. E. Running and tumbling with *E. coli* in polymeric solutions. *Scientific reports* **5**, 15761, doi:10.1038/srep15761 (2015).

45 Schade, S. Z., Adler, J. & Ris, H. How bacteriophage chi attacks motile bacteria. *J Virol* **1**, 599-609 (1967).

46 Meynell, E. W. A phage, phi-chi, which attacks motile bacteria. *Journal of General Microbiology* **25**, 253-& (1961).

47 Samuel, A. D. T., Pitta, T. P., Ryu, W. S., Danese, P. N., Leung, E. C. W. & Berg, H. C. Flagellar determinants of bacterial sensitivity to chi-phage. *Proceedings of the National Academy of Sciences of the United States of America* **96**, 9863-9866, doi:DOI 10.1073/pnas.96.17.9863 (1999).

48 Chaturongakul, S. & Ounjai, P. Phage-host interplay: examples from tailed phages and Gram-negative bacterial pathogens. *Front Microbiol* **5**, 442, doi:10.3389/fmicb.2014.00442 (2014).

49 Scharf, B., Schuster-Wolff-Buhring, H., Rachel, R. & Schmitt, R. Mutational analysis of the *Rhizobium lupini* H13-3 and *Sinorhizobium meliloti* flagellin genes: importance of flagellin A for flagellar filament structure and transcriptional regulation. *J Bacteriol* **183**, 5334-5342 (2001).

50 Parkinson, J. S. Complementation analysis and deletion mapping of *Escherichia coli* mutants defective in chemotaxis. *J Bacteriol* **135**, 45-53 (1978).

bioRxiv preprint doi: https://doi.org/10.1101/691568; this version posted July 3, 2019. The copyright holder for this preprint (which was not certified by peer review) is the author/funder, who has granted bioRxiv a license to display the preprint in perpetuity. It is made available under aCC-BY 4.0 International license.

51 Armstrong, J. B., Adler, J. & Dahl, M. M. Nonchemotactic mutants of *Escherichia coli*. *J Bacteriol* **93**, 390-398 (1967).

52 Jacob, F. & Wollman, E. L. Etude genetique d'un bacteriophage tempere d'Escherichia coli. III. Effet du rayonnement ultraviolet sur la recombinaison genetique. *Annales de l'Institut Pasteur* **88**, 724-749 (1955).

53 Swiecicki, J. M., Sliusarenko, O. & Weibel, D. B. From swimming to swarming: *Escherichia coli* cell motility in two-dimensions. *Integr Biol (Camb)* **5**, 1490-1494, doi:10.1039/c3ib40130h (2013).

54 Ma, Y. G., Zhu, C. Y., Ma, P. S. & Yu, K. T. Studies on the diffusion coefficients of amino acids in aqueous solutions. *J Chem Eng Data* **50**, 1192-1196, doi:10.1021/je049582g (2005).

55 Gallet, R., Kannoly, S. & Wang, I. N. Effects of bacteriophage traits on plaque formation. *Bmc Microbiology* **11**, doi:10.1186/1471-2180-11-181 (2011).

56 Shao, Y. & Wang, I. N. Bacteriophage adsorption rate and optimal lysis time. *Genetics* **180**, 471-482, doi:10.1534/genetics.108.090100 (2008).

57 Shao, Y. & Wang, I. N. Effect of late promoter activity on bacteriophage lambda fitness. *Genetics* **181**, 1467-1475, doi:10.1534/genetics.108.098624 (2009).

58 De Paepe, M. & Taddei, F. Viruses' life history: towards a mechanistic basis of a trade-off between survival and reproduction among phages. *PLoS Biol* **4**, e193, doi:10.1371/journal.pbio.0040193 (2006).

bioRxiv preprint doi: https://doi.org/10.1101/691568; this version posted July 3, 2019. The copyright holder for this preprint (which was not certified by peer review) is the author/funder, who has granted bioRxiv a license to display the preprint in perpetuity. It is made available under aCC-BY 4.0 International license.

Supplementary Materials

Formation of Phage Lysis Patterns and Implications on Co-Propagation of Phages and Motile Host Bacteria

Xiaochu Li, Floricel Gonzalez, Nathaniel Esteves, Birgit E. Scharf, Jing Chen

bioRxiv preprint doi: https://doi.org/10.1101/691568; this version posted July 3, 2019. The copyright holder for this preprint (which was not certified by peer review) is the author/funder, who has granted bioRxiv a license to display the preprint in perpetuity. It is made available under aCC-BY 4.0 International license.

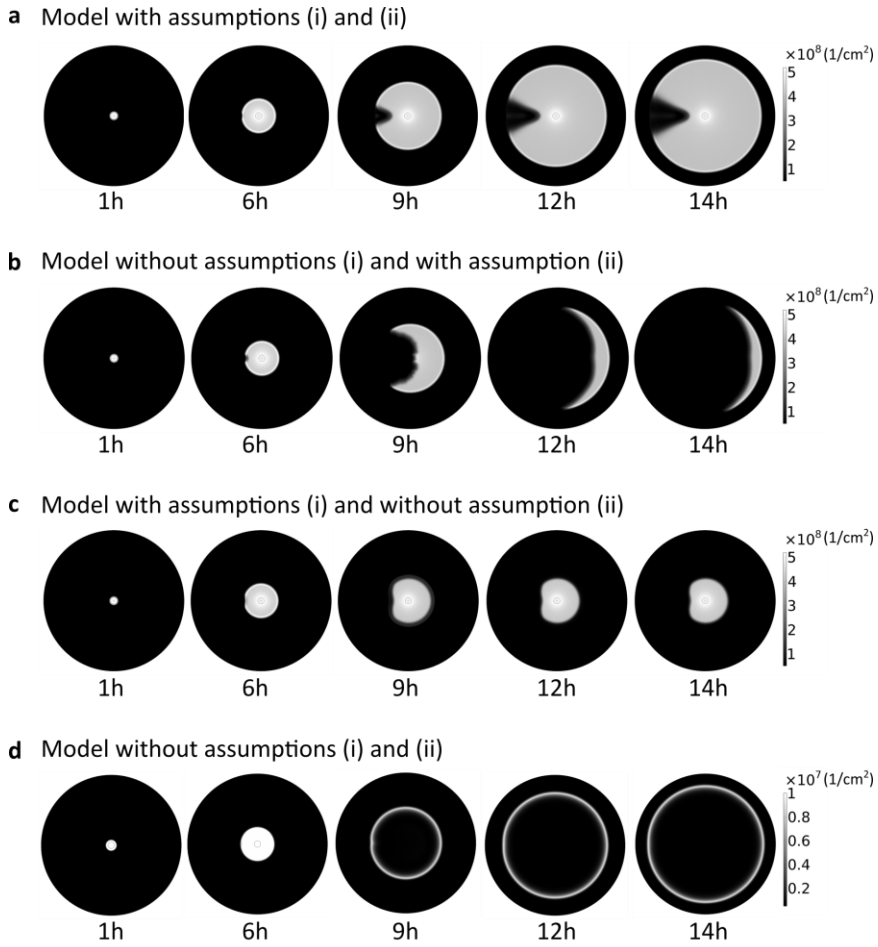

S1 Fig. Both direct and indirect negative dependences of phage proliferation on bacterial density are necessary for generating straight radial boundaries in the lysis pattern. (a) Simulated lysis pattern formation with both Assumptions (i) and (ii). Same results as Fig. 1b, second row. (b) Simulated lysis pattern formation without Assumption (i), but with Assumption (ii). (c) Simulated lysis pattern formation without Assumption (ii), but with Assumption (i). (d) Simulated lysis pattern formation without both Assumptions. As described in Results, Assumption (i) states that nutrient deficiency inhibits phage replication, and Assumption (ii) states that high bacterial density inhibits phage production.

bioRxiv preprint doi: https://doi.org/10.1101/691568; this version posted July 3, 2019. The copyright holder for this preprint (which was not certified by peer review) is the author/funder, who has granted bioRxiv a license to display the preprint in perpetuity. It is made available under aCC-BY 4.0 International license.

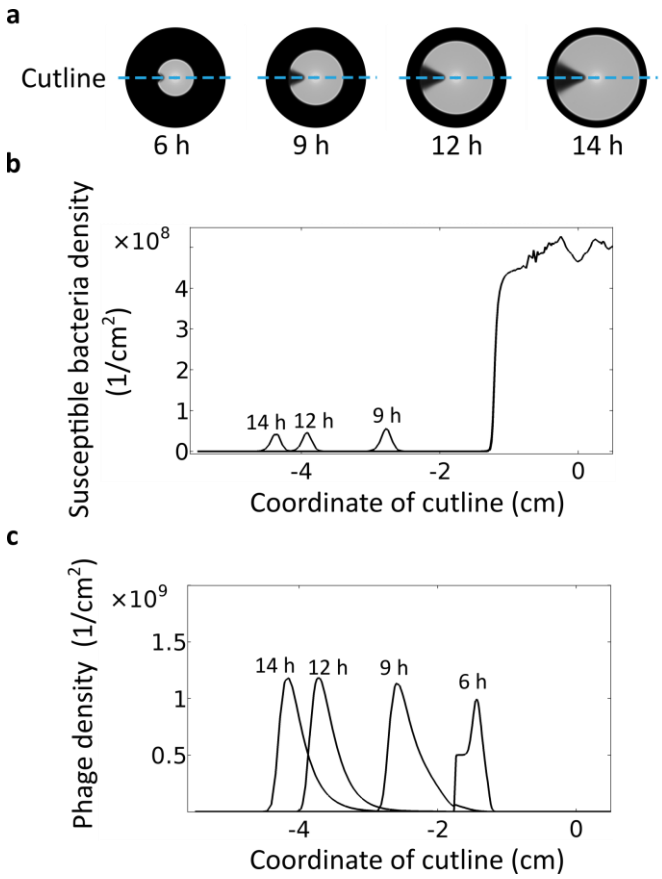

S2 Fig. Model results show steady bacteria and phage densities at the expanding front after the phage initiation zone emerges. (a) Lysis patterns over time. Blue dashed line: cutline over which the density profiles are plotted in (b). (b) Density profiles of susceptible bacteria over the cutline at the labeled times. (c) Density profiles of phages over the cutline at the labeled times.

bioRxiv preprint doi: https://doi.org/10.1101/691568; this version posted July 3, 2019. The copyright holder for this preprint (which was not certified by peer review) is the author/funder, who has granted bioRxiv a license to display the preprint in perpetuity. It is made available under aCC-BY 4.0 International license.

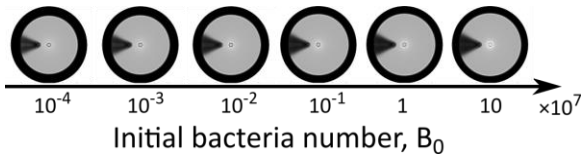

S3 Fig. Simulation results with various numbers of inoculated bacteria.

bioRxiv preprint doi: https://doi.org/10.1101/691568; this version posted July 3, 2019. The copyright holder for this preprint (which was not certified by peer review) is the author/funder, who has granted bioRxiv a license to display the preprint in perpetuity. It is made available under aCC-BY 4.0 International license.

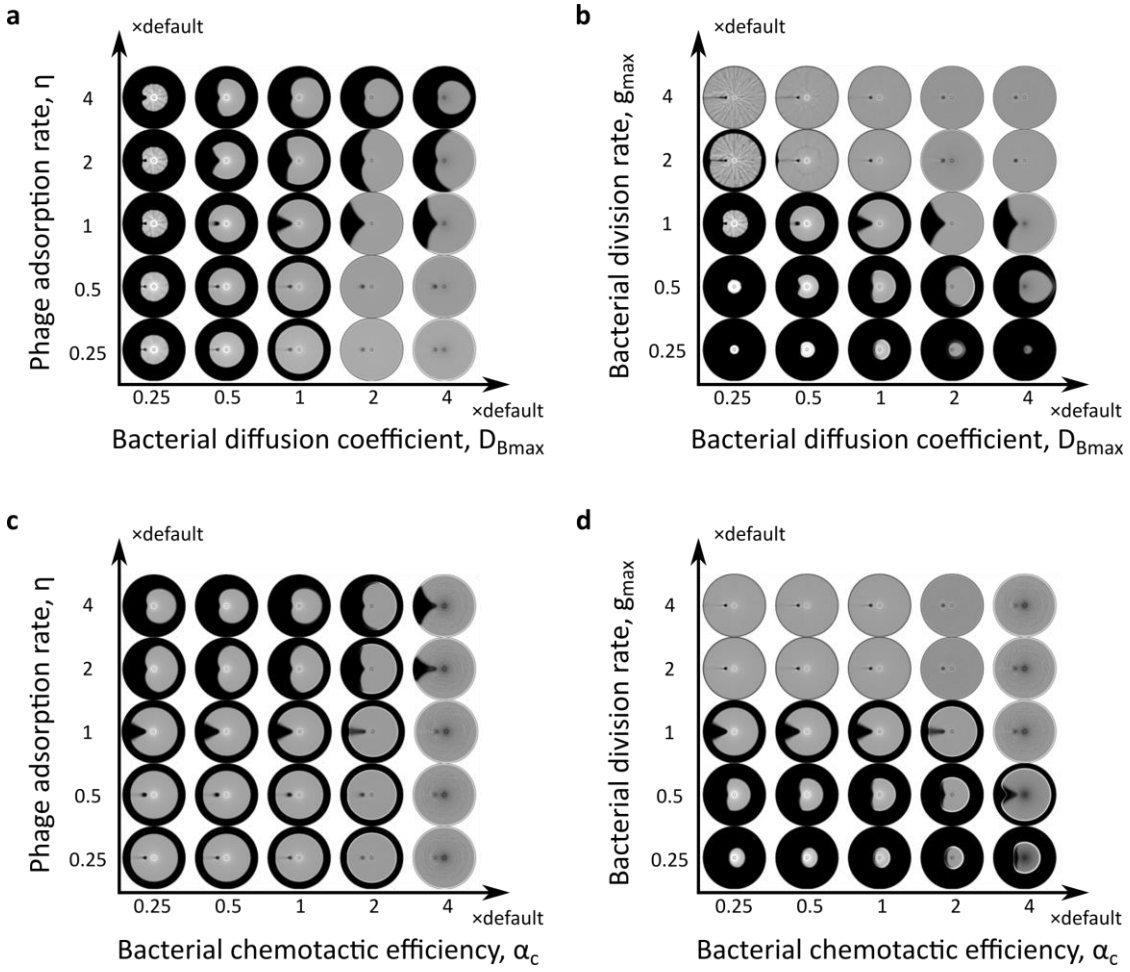

S4 Fig. Lysis pattern with straight radial boundaries requires balance between intrinsic properties of bacteria and phage. Simulated lysis patterns with (a) various phage adsorption rate constants and bacterial diffusion coefficients, (b) various bacterial division rate constants and bacterial diffusion coefficients, (c) various phage adsorption rate constants and chemotactic efficiencies, and (d) various bacterial division rate constants and chemotactic efficiencies.

bioRxiv preprint doi: https://doi.org/10.1101/691568; this version posted July 3, 2019. The copyright holder for this preprint (which was not certified by peer review) is the author/funder, who has granted bioRxiv a license to display the preprint in perpetuity. It is made available under aCC-BY 4.0 International license.

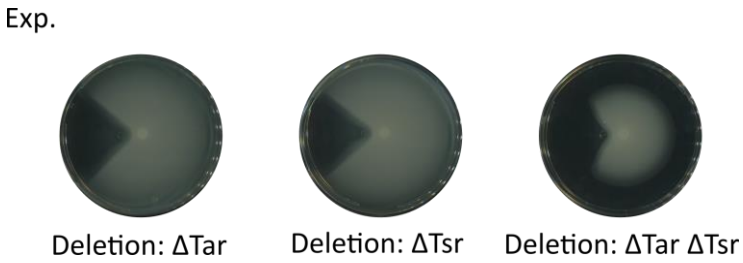

S5 Fig. Experimental results of *S*. Typhimurium strains lacking chemoreceptors.

bioRxiv preprint doi: https://doi.org/10.1101/691568; this version posted July 3, 2019. The copyright holder for this preprint (which was not certified by peer review) is the author/funder, who has granted bioRxiv a license to display the preprint in perpetuity. It is made available under aCC-BY 4.0 International license.

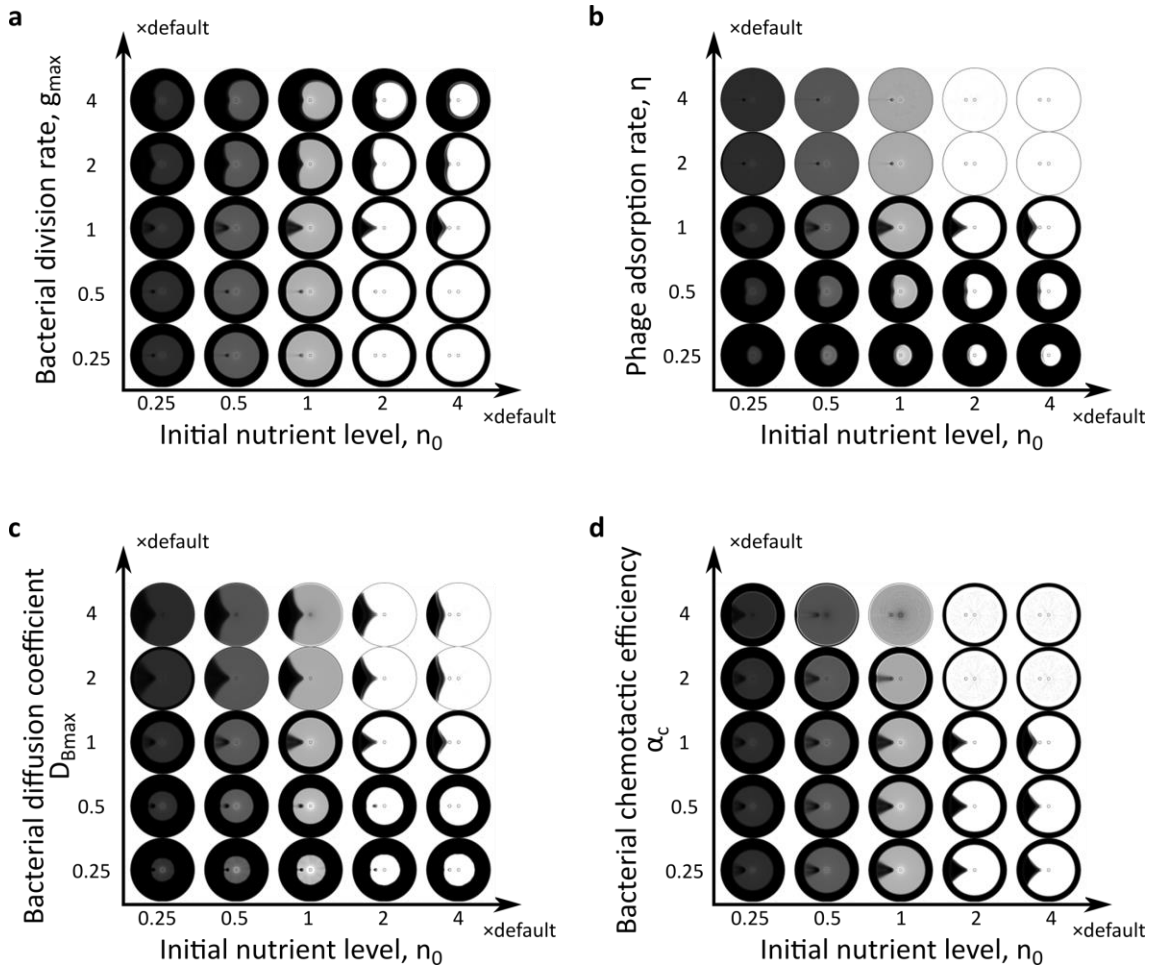

S6 Fig. The shape of lysis area depends on the competition between phages and bacteria, but not the initial nutrient level. Simulated lysis patterns with various initial nutrient levels and (a) bacterial division rate constants, (b) phage adsorption rate constants, (c) bacterial diffusion coefficients, (d) chemotactic efficiencies.

bioRxiv preprint doi: https://doi.org/10.1101/691568; this version posted July 3, 2019. The copyright holder for this preprint (which was not certified by peer review) is the author/funder, who has granted bioRxiv a license to display the preprint in perpetuity. It is made available under aCC-BY 4.0 International license.

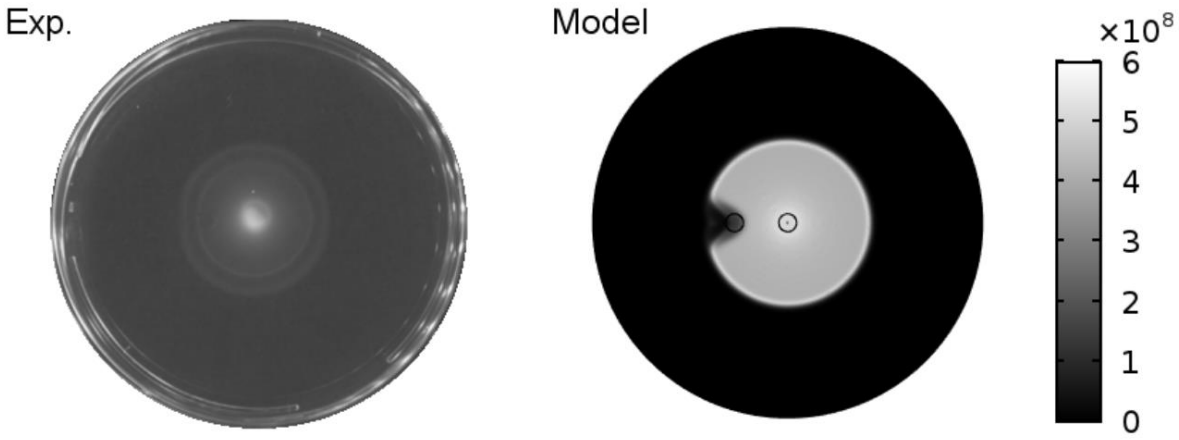

S1 Movie. Time evolution of the lysis pattern in experiment and model. Each frame displays corresponding time points in experiment vs. model. Total time 14 hrs. Color bar represents density of bacteria (cm^{-2}) in model.

bioRxiv preprint doi: https://doi.org/10.1101/691568; this version posted July 3, 2019. The copyright holder for this preprint (which was not certified by peer review) is the author/funder, who has granted bioRxiv a license to display the preprint in perpetuity. It is made available under aCC-BY 4.0 International license.

Mean field model for bacterial diffusion and chemotaxis with nutrient dependent motility

Here we derive the mean-field diffusion and chemotaxis terms, following the original work by Keller and Segel [1]. Specifically our model incorporates a nonlinear dependence of bacterial motility on nutrient level (as bacteria require energy to move). Note that both the diffusion and chemotaxis flux terms result from the run-and-tumble process of the bacteria; hence any regulation of bacterial motility or tumbling would affect both terms. Our derivation below emphasizes such quantitative relation between the diffusion and chemotaxis fluxes. For simplicity we derive the flux terms in 1D space, and the result can be readily generalized to 2D space. Our derivation is based on the following assumptions.

(1) The bacterium takes left or right steps of length Δ.

(2) The original paper by Keller and Segel assumes that the average frequency of steps to the left is governed by the mean nutrient concentration at the left edge, and vice versa [1]. Hence the difference in nutrient concentration across the cell body length governs the chemotaxis flux. This gradient sensing mode, however, differs from the temporal mode exploited by real bacteria [2]. Instead of detecting the difference of nutrient concentration at two ends of the cell (which is too small for reliable gradient detection in a tiny bacterial cell), the bacterial chemoreceptors use molecular memory to detect the temporal increase or decrease of nutrient signals as the bacterium swims [3]. However, note that the cell body length pictured in Keller and Segel' original derivation essentially reflects the distance over which nutrient gradient is detected. Therefore, if we simply generalize the cell body to a "gradient-sensing distance", the same derivation will apply to the temporal mode of gradient sensing (Fig. S7). In the temporal mode, the gradient-sensing distance reflects the distance a bacterium swims in the characteristic time of chemoreceptor memory.

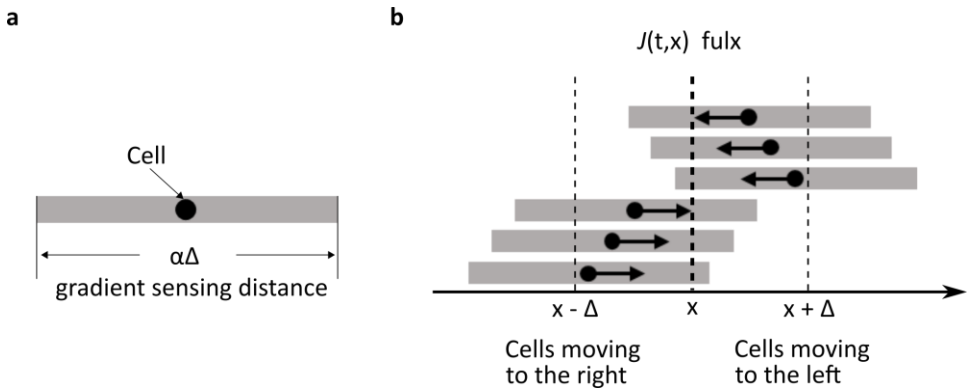

S7 Fig. Spatial flux of bacteria. (a) Generalization of cell body length in the Keller-Segel derivation to gradient-sensing distance. (b) Illustration of the bacterial flux through a spatial location x. The flux of right-moving cells (lower batch) passing through the location x in a single step is the integration of the product of the step frequency to the right and cell density over the interval $[x-\Delta, x]$ (first integration term in Eq. (S1)). Vice versa, the flux of left-moving cells (upper batch) going through the location x in a single step is the integration of the product of the step frequency to the left and cell density over the interval $[x, x+\Delta]$ (second integration term in Eq. (S1)).

bioRxiv preprint doi: https://doi.org/10.1101/691568; this version posted July 3, 2019. The copyright holder for this preprint (which was not certified by peer review) is the author/funder, who has granted bioRxiv a license to display the preprint in perpetuity. It is made available under aCC-BY 4.0 International license.

Let $B(t,x)$ denote bacterial density at time t and location$x$. Let $f(n)$ denote the average frequency of steps in a given direction, which is dependent on the local nutrient concentration, $n(t,x)$. α is the ratio of the gradient-sensing distance to the step size. For a bacterium centered at location x, its frequencies of steps to the right and left, according to the 2nd assumption above, depend on the nutrient level at the right and left end of the gradient-sensing distance, i.e., written as $f[n(t,x+\frac{1}{2}\alpha\Delta)]$ and $f[n(t,x-\frac{1}{2}\alpha\Delta)]$, respectively. The net flux of bacteria $J(t,x)$ at time t and location x (Fig. S9b) is defined by the amount of bacteria per unit time moving to the right minus the amount of bacteria per unit time moving to the left [1] (Eq.(S1)).

$$J(t,x)=\int_{x-\Delta}^{x} f\left[n(t,s+\frac{1}{2}\alpha\Delta)\right]B(t,s)ds-\int_{x}^{x+\Delta} f\left[n(t,s-\frac{1}{2}\alpha\Delta)\right]B(t,s)ds \quad \text{(S1)}$$

Note that when the step length Δ is sufficiently small, we can approximate the flux term up to $O(\Delta^2)$, as shown in Eqs.(S2) and (S3).

$$\begin{aligned}\int_{x-\Delta}^{x} f\left[n(t,s+\frac{1}{2}\alpha\Delta)\right]B(t,s)ds \\ \approx f[n(t,x)]B(t,x)\Delta-\frac{f(t,x)\partial_x B(t,x)}{2}\Delta^2 \\ +\frac{f'[n(t,x)]\partial_x n(t,x)B(t,x)}{2}[\Delta x+\Delta^2(\alpha-1)]\end{aligned} \quad \text{(S2)}$$

$$\begin{aligned}\int_{x}^{x+\Delta} f\left[n(t,s-\frac{1}{2}\alpha\Delta)\right]B(t,s)ds \\ \approx f[n(t,x)]b(t,x)\Delta+\frac{f(t,x)\partial_x B(t,x)}{2}\Delta^2 \\ -\frac{f'[n(t,x)]\partial_x n(t,x)B(t,x)}{2}[-\Delta x+\Delta^2(\alpha-1)]\end{aligned} \quad \text{(S3)}$$

Plugging Eqs.(S2) and (S3) into Eq.(S1) yields

$$J(t,x)=-\Delta^2 f(n)\partial_x B(t,x)+(\alpha-1)\Delta^2 f'(n)\partial_x n(t,x)B(t,x) \quad \text{(S4)}$$

The first term describes diffusion (random motion) of the cells, and the second one describes the chemotaxis (biased motion up the nutrient gradient).

Because bacteria require energy to move, the cell velocity is likely an increasing function of nutrient level with a maximum value. We assumed a Michaelis-Menten type relation between nutrient level and cell velocity. Because $f(n)$ is proportional to the cell velocity, it is also a Michaelis-Menten function of nutrient level (Eq. (S5)).

$$f=\frac{n}{n+K_c} \quad \text{(S5)}$$

where K_c is the nutrient level that allows half maximum cell velocity.

bioRxiv preprint doi: https://doi.org/10.1101/691568; this version posted July 3, 2019. The copyright holder for this preprint (which was not certified by peer review) is the author/funder, who has granted bioRxiv a license to display the preprint in perpetuity. It is made available under aCC-BY 4.0 International license.

From Eq.(S4), we obtain the effective diffusion coefficient as a function of local nutrient level (Eq.(S6)).

$$D_B(n) \equiv \Delta^2 f(n) = D_{Bmax} \frac{n}{n + K_c} \tag{S6}$$

where the maximum diffusion coefficient, D_{Bmax}, reflects maximum bacterial motility.

From Eq.(S4) we also obtain the chemotactic coefficient $\chi(n)$ (Eq.(S7)).

$$\chi(n) = (\alpha - 1)\Delta^2 f'(n) \tag{S7}$$

which can be rewritten as

$$\chi(n) = \alpha_c D_{Bmax} \frac{K_c}{(n + K_c)^2} \tag{S8}$$

where $\alpha_c = \alpha - 1$ represents the chemotactic efficiency. Note that the chemotactic coefficient given in Eq.(S8) is similar to that in the classic Keller-Segel models [4]. However, instead of representing a saturated chemotactic response, the fraction term in Eq.(S8) represents the saturation of cell velocity, with increasing nutrient level, as a related fraction term also appears in the diffusion flux (Eq.(S6)).

The overall spatial flux of bacteria in 2D space, including random motion and chemotaxis process, is derived by replacing the 1D spatial derivative, ∂_x, by the 2D gradient operator, $\nabla = [\partial_x, \partial_y]$ (Eq.S(9)).

$$J_B = -D_B(n)\nabla b + \chi(n) b \nabla n \tag{S9}$$

Supplementary References

1. Keller EF, Segel LA. Model for chemotaxis. J Theor Biol. 1971;30(2):225-34.
2. Vladimirov N, Sourjik V. Chemotaxis: how bacteria use memory. Biol Chem. 2009; 390(11):1097-104.
3. Wadhams GH, Armitage JP. Making sense of it all: bacterial chemotaxis. Nat Rev Mol Cell Biol. 2004;5(12):1024-37.
4. Lapidus IR, Schiller R. Model for the chemotactic response of a bacterial population. Biophys J. 1976;16(7):779-89.